that all the structure factors, recalculated for the (*B*) species and different Miller indices, are *identical*, in magnitudes and phases, to those calculated when it was thought the crystal was of type (*A*). Repeating the computations for an (*A*) crystal with the same Miller indices ($\bar{3}30$ for the main reflection, $\bar{6}2\bar{6}$ and $\bar{1}3\bar{6}$ for the simultaneous reflections) will give different results, as in the previous case, with a peak intensity equal to I_4. However, the peak intensities found now are identical to those found earlier ($I_1 = I_3$, $I_2 = I_4$), since all the structure factors are rigorously identical when switching from one space group to another and changing the Miller indices accordingly.

It should be stressed that anomalous dispersion does not help here, as in the previous case. Our calculations were performed with large unrealistic values for the imaginary components of the scattering factors and the equality expressed in (1) was always found to be rigorously true, to within computer accuracy.

The situation is quite different in high-energy electron diffraction ($E = 30$–50 keV or higher). In this case, inelastic scattering (plasmon scattering, single-electron excitations, thermal diffuse scattering and radiation losses) is responsible for a substantial imaginary part of the Fourier components of the crystal potential, typically 10% of the real part, even with light atoms. In such a situation the absolute determination of polarity and enantiomorphism is always possible. Multiple diffraction, in this case, is not an essential ingredient, but rather an unavoidable feature, necessitated by the geometry of the diffraction process (see, for example, the paper by Taftø & Spence, 1982). The situation is reviewed in a recent book by Spence & Zuo (1992).

In conclusion, multiple-beam diffraction cannot resolve the enantiomorphism problem and does not help in solving the polarity problem of acentric crystals in comparison with standard two-beam experiments, in which anomalous-dispersion effects are exploited to differentiate between Friedel pairs.

In view of the analysis given in this paper, the results presented by Chang, King, Huang & Gao (1991) and by Hümmer, Weckert & Bondza (1989) are somewhat questionable.

This work was supported by the National Science Foundation, grant no. DMR-9108684.

References

Chang, S. L., King, H. E. Jr, Huang, M. T. & Gao, Y. (1991). *Phys. Rev. Lett.* **67**, 3113–3116.

Colella, R. (1974). *Acta Cryst.* A**30**, 413–423.

De Vries, A. (1958). *Nature (London)*, **181**, 1193.

Hümmer, K., Weckert, E. & Bondza, H. (1989). *Acta Cryst.* A**45**, 182–187.

Shen, Q. (1984). PhD Proposal. Purdue Univ., Indiana, USA. (Unpublished.)

Shen, Q. (1986). *Acta Cryst.* A**42**, 525–533.

Shen, Q. & Colella, R. (1986). *Acta Cryst.* A**42**, 533–538.

Spence, J. C. H. & Zuo, J. M. (1992). *Electron Microdiffraction.* New York: Plenum Press.

Taftø, J. & Spence, J. C. H. (1982). *J. Appl. Cryst.* **15**, 60–64.

Acta Cryst. (1994). A**50**, 57–63

Thermal Diffuse Scattering in Time-of-Flight Neutron Diffractometry

By N. C. Popa

Institute of Physics and Technology of Materials, PO Box MG-7, Bucharest, Romania

and B. T. M. Willis

Chemical Crystallography Laboratory, University of Oxford, 9 Parks Road, Oxford OX1 3PD, England

(*Received* 21 *October* 1992; *accepted* 22 *June* 1993)

Abstract

The coherent one-phonon scattering cross section measured in time-of-flight (TOF) neutron diffractometry is derived for any ratio between the sample-to-detector flight path and the total flight path. For the particular case of scattering by acoustic phonons in monocrystals, the differential cross section is described in terms of the scattering surface in four-dimensional space ($\mathbf{Q}_e,\omega$), where $\hbar\mathbf{Q}_e$ is the momentum transfer for elastic scattering and $\hbar\omega$ is the energy transfer. This cross section is required in calculating the thermal diffuse scattering (TDS) correction for TOF neutron diffractometry.

1. Introduction

The problem of the TDS correction of Bragg peaks was solved many years ago for X-ray diffraction (Cooper & Rouse, 1968) and for the fixed-wavelength method of neutron diffraction (Willis, 1970; Cooper, 1971). The calculation of the TDS correction for the neutron time-of-flight (TOF) case is more complicated than for the fixed-wavelength case.

In this paper, we consider some features of the differential scattering cross section that are important in calculating the TDS correction factor for TOF experiments in neutron diffraction. In a subsequent paper, we shall calculate the magnitude of the correction itself.

We shall show that there is one surface in $(\mathbf{Q}_e,\omega)$ space for each acoustic mode of vibration, where $\hbar\mathbf{Q}_e$ is the momentum transfer for elastic scattering and $\hbar\omega$ is the energy transfer (here, $\hbar = h/2\pi$). By crossing this surface with a plane in three-dimensional $\mathbf{Q}_e$ space, normal to the scattering plane, we obtain a surface having different topologies for three regions of the quantity β, representing the ratio of the sound velocity in the crystal to the velocity of Bragg-scattered neutrons. The limiting values, β_ν and β_μ $(\beta_\nu \le \beta_\mu)$, separating these regions are functions of ξ and the Bragg angle θ_B, where ξ is the ratio between the sample-to-detector flight path and the total flight path. In addition, β_μ depends on the orientation of the crossing plane.

2. The differential cross section measured in TOF neutron diffractometry

A neutron or X-ray diffractometer is used to determine the structure of condensed matter by measuring the differential cross section for elastic coherent scattering. This scattering is a function of the position in reciprocal space $\mathbf{Q}$, which is uniquely determined for any diffractometer setting. However, inelastic scattering also exists, which is recorded in the detector at the same setting and the diffractometer is unable to determine the energy transfer $\hbar\omega$ for this inelastic scattering. The diffractometer cannot localize each point in four-dimensional space $(\mathbf{Q},\omega)$, but can only integrate the contributions to the counting rate from all points in this space situated on a given curve, Γ: $[\mathbf{Q}(\omega),\omega]$. A particular point on this curve is $\mathbf{Q}_e = [\mathbf{Q}(0),0]$, which corresponds to elastic scattering. The shape of Γ depends on the diffraction method used. Let us find Γ for TOF neutron diffraction.

2.1. *Integration path in* $(\mathbf{Q},\omega)$ *space*

We firstly denote the time of flight of the elastically scattered neutrons by T_e. In the same time channel, the inelastically scattered neutrons are also counted, for which the times of flight before (T_1) and after (T_2) scattering fulfil the condition

$$T_1 + T_2 = T_e. \tag{1}$$

With the relation between the energy E_i $(i = 1, 2, e)$ and the time of flight T_i taken into account, (1) becomes

$$E_2 = E_1\psi(E_1/E_e),$$

where

$$\psi(E_1/E_e) = (L_2^2/L^2)/[(E_1/E_e)^{1/2} - L_1/L]^2. \tag{2}$$

The following condition is also fulfilled:

$$E_eL_1^2/L^2 \le E_1 < \infty.$$

Here, L_1 and L_2 are the flight paths before and after scattering and $L = L_1 + L_2$.

Secondly, denoting by $\mathbf{i}_1$, $\mathbf{i}_2$ the unit vectors along the incident and scattering directions, respectively, one has

$$\begin{aligned}\mathbf{Q} &= \mathbf{k}_2 - \mathbf{k}_1\\ &= k_e(E_1/E_e)^{1/2}[\psi(E_1/E_e)\mathbf{i}_2 - \mathbf{i}_1],\end{aligned}$$

where $\mathbf{k}_i$ is the neutron wave vector corresponding to E_i and k_e is the wave number of the elastically scattered neutrons. This equation together with the equation

$$\hbar\omega = E_2 - E_1 = E_1[\psi(E_1/E_e) - 1]$$

are the parametric equations (parameter E_1) of the integration curve Γ. This curve passes through the reciprocal-space point $\mathbf{Q}_e$,

$$\mathbf{Q}_e = k_e(\mathbf{i}_2 - \mathbf{i}_1).$$

2.2. *Measured differential cross section*

Now we can write the counting rate of the neutrons scattered in the solid angle $d\Omega$ and in the time interval dT_e (to which the energy interval dE_e corresponds):

$$\begin{aligned}dN\,dE_e = d\Omega\,dT_e \int_{E_eL_1^2/L^2}^{\infty} dE_1\Phi(E_1)\\ \times [A(E_1,E_2)\,d^2\sigma/d\Omega\,dT_2],\end{aligned} \tag{3}$$

where $E_2 = E_1\psi(E_1/E_e)$. Here, $\Phi(E_1)$ is the incident flux and $A(E_1,E_2)$ is a factor that includes the transmission in air and the sample and the detector efficiency. By definition, the differential cross section is

$$d\sigma/d\Omega = (dN/d\Omega)[\Phi(E_e)A(E_e,E_e)]^{-1}. \tag{4}$$

Taking into account the relation

$$(dT_e/dE_e)(dE_2/dT_2) = (L/L_2)(E_2/E_e)^{3/2}$$

and using the notation

$$F(E_1,E_2) = \Phi(E_1)A(E_1,E_2)/\Phi(E_e)A(E_e,E_e),$$
$$z = E_1/E_e, \quad \xi = L_2/L,$$

one obtains from (3) and (4) the equation

$$\mathrm{d}\sigma/\mathrm{d}\Omega = (E_e/\xi)\int_{(1-\xi)^2}^{\infty} \mathrm{d}z\, z^{3/2}\psi(z)^{3/2} \times [F(E_1,E_2)\,\mathrm{d}^2\sigma/\mathrm{d}\Omega\,\mathrm{d}E_2], \quad (5)$$

where $E_1 = E_e z$; $E_2 = E_e z\psi(z)$. This is the differential cross section measured by the TOF diffractometer.

The function

$$\psi(z) = \xi^2/(z^{1/2} - 1 + \xi)^2$$

is represented in Fig. 1 for two values of ξ. It becomes infinite for $z = (1-\xi)^2$: this discontinuity is an integrable one but, unfortunately, it produces a large rounding error in the numerical integration of (5). Another difficulty appears if we want to find the limit of $\mathrm{d}\sigma/\mathrm{d}\Omega$ as $\xi \to 0$. (Most, but not all, TOF diffractometers operate with ξ close to zero.) Thus, the function $\psi(z)$ is continuous in the range $[(1-\xi)^2, \infty]$ but is not uniform; this fact prohibits the insertion of the limit before the evaluation of the integral in (5).

Both difficulties can be removed by changing the integration variable to w, where

$$w = \hbar\omega/E_e.$$

Equation (5) then becomes

$$\frac{\mathrm{d}\sigma}{\mathrm{d}\Omega} = E_e \int_{-\infty}^{\infty} \mathrm{d}w \frac{z(w)[z(w)+w]^{3/2}}{\{[z(w)+w]^{3/2} - \xi w\}} \times \left[F(E_1,E_2)\frac{\mathrm{d}^2\sigma}{\mathrm{d}\Omega\,\mathrm{d}E_2}\right], \quad (6)$$

where $E_1 = E_e z(w)$; $E_2 = E_e[z(w) + w]$. The function $z(w)$ is obtained by numerically solving the equation

$$w = z[\psi(z) - 1].$$

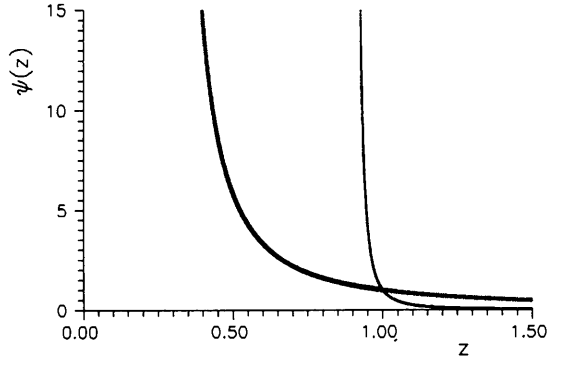

Fig. 1. The function $\psi(z)$ for two values of ξ: $\xi = 0.5$ (thick curve) and $\xi = 0.05$ (thin curve).

In the range $(-\infty, \infty)$, $z(w)$ is continuous and has the following asymptotic lines:

$$\underset{w\to-\infty}{z(w)} = -w + \xi^2; \quad \underset{w\to\infty}{z(w)} = (1-\xi)^2.$$

For $\xi \to 0$, the function $z(w)$ becomes identical with its asymptotes.

The cross section is

$$\mathrm{d}\sigma/\mathrm{d}\Omega = E_e \int_{-1}^{\infty} \mathrm{d}w[F_0(E_1,E_2)\,\mathrm{d}^2\sigma/\mathrm{d}\Omega\,\mathrm{d}E_2], \quad (7)$$

where $E_1 = E_e$; $E_2 = E_e(1+w)$ and

$$F_0(E_1,E_2) = A(E_1,E_2)/A(E_e,E_e).$$

Hence, provided that the flight path from the sample to the detector is much smaller than the total flight path, the TOF diffractometer integrates the inelastic processes, for a given energy of the incident neutrons, in the same way as the angular-dispersive diffractometer.

3. The TDS differential cross section

Let us now apply (5) to the scattering by acoustic phonons in monocrystals. Following Marshall & Lovesey (1971), the one-phonon double-differential cross section is

$$\mathrm{d}^2\sigma/\mathrm{d}\Omega\,\mathrm{d}E_2 = [(2\pi)^3/v_c](F_Q^2/2M_c)(k_2/k_1) \times \sum_{j=1}^{3}\sum_{\mathbf{q}}[|\mathbf{Q}\cdot\boldsymbol{\sigma}_j(\mathbf{q})|^2/\omega_j(\mathbf{q})] \times \sum_{\varepsilon=\pm1}\{n[\omega_j(\mathbf{q})] + 1/2 + \varepsilon/2\} \times \delta[\omega + \varepsilon\omega_j(\mathbf{q})]\delta(\mathbf{Q} - 2\pi\mathbf{H} - \mathbf{q}), \quad (8)$$

where v_c and M_c are the unit-cell volume and mass, F_Q is the structure factor, $\mathbf{H}$ is a Bragg vector, $\boldsymbol{\sigma}_j(\mathbf{q})$ and $\omega_j(\mathbf{q})$ are the polarization vector and frequency of the mode $(j,\mathbf{q})$, respectively, $\mathbf{q}$ being the phonon wave vector and j the branch of the dispersion relation. $n(\omega)$ is the Bose factor and ε is $+1$ for phonon creation and -1 for phonon annihilation.

Firstly, we perform the summation over $\mathbf{q}$ in (8) and then the integral over E_1 (in practice over k_1 as $\mathrm{d}E_1 = \hbar^2 m_n^{-1} k_1 \mathrm{d}k_1$, m_n being the neutron mass). One obtains

$$\mathrm{d}\sigma/\mathrm{d}\Omega = (V/v_c)F_Q^2(\hbar/2M_c)(L/L_2) \times \sum_{j=1}^{3}\sum_{\varepsilon=\pm1}\sum_{n} F(k_{1n}/k_e)^2[\varphi(k_{1n}/k_e)]^2 \times |\mathbf{Q}_n\cdot\boldsymbol{\sigma}_j(\mathbf{q}_n)|^2/\omega_j(\mathbf{q}_n) \times \{n[\omega_j(\mathbf{q}_n)] + (\varepsilon+1)/2\} \times |1 + [\varphi(k_{1n}/k_e)]^{3/2} + (m_n\varepsilon/\hbar k_{1n})[\mathbf{i}_1 + \varphi(k_{1n}/k_e)(L_1/L_2)\mathbf{i}_2] \times \mathrm{grad}_{\mathbf{q}}\,\omega_n(\mathbf{q}_n)|^{-1}. \quad (9)$$

In this expression, V is the sample volume and k_{1n} is the nth root of the following equation with the variable k_1,

$$k_1^2[\varphi(k_1/k_e)-1]+(2m_n/\hbar)\varepsilon\omega_j(\mathbf{q})=0, \qquad (10)$$

where

$$\mathbf{q}=\mathbf{Q}-2\pi\mathbf{H}=\mathbf{k}_2-\mathbf{k}_1-2\pi\mathbf{H}$$

and

$$k_2=k_1\varphi(k_1/k_e). \qquad (11)$$

The function φ in (9), (10) and (11) is ψ, as defined in (2), but with E replaced by $\hbar^2k^2/2m_n$:

$$\varphi(k_1/k_e)=\xi^2/(k_1/k_e-1+\xi)^2. \qquad (12)$$

Let us now introduce some conventional approximations to simplify (9).

(*a*) We are interested in small q so that $\mathbf{Q}\simeq 2\pi\mathbf{H}$. The energy transfer is also small; then, $k_1\simeq k_e$, $\varphi\simeq 1$ and $F\simeq 1$. For small q, the dispersion relation is $\omega_j(\mathbf{q})=c_jq$, c_j being the sound velocity in the crystal, a quantity dependent on the direction of propagation of the acoustic wave and on its direction of polarization.

(*b*) We use the two-velocity approximation (Willis, 1969), stating that all the acoustic waves are pure longitudinal and pure transverse, with the phase velocities, c_1 (longitudinal) and c_2 (transverse), independent of direction. As a consequence, $\mathrm{grad}_q\ \omega_j(\mathbf{q})=c_j(\mathbf{q}/q)$; on the other hand, the sum over $j=1,3$ in (9) reduces to a sum of two terms, the first being proportional to $|\mathbf{Q}\cdot\boldsymbol{\sigma}_1(\mathbf{q})|^2\simeq 4\pi^2H^2\cos^2\rho$ and the second to $|\mathbf{Q}\cdot\boldsymbol{\sigma}_2(\mathbf{q})|^2+|\mathbf{Q}\cdot\boldsymbol{\sigma}_3\mathbf{q})|^2\simeq 4\pi^2H^2\sin^2\rho$, where ρ is the angle between $\mathbf{Q}$ and $\mathbf{q}$. Furthermore, $\cos^2\rho$ and $\sin^2\rho$ are replaced by their average values, 1/3 and 2/3, respectively.

(*c*) The high-temperature approximation is also invoked, so that $\hbar\omega<<K_BT$, where K_B is Boltzmann's constant. In this case,

$$n(\omega)=[\exp(\hbar\omega/K_BT)-1]^{-1}\simeq K_BT/\hbar\omega>>1$$

and we can neglect $(\varepsilon+1)/2$.

After these approximations are made, (9) becomes

$$\mathrm{d}\sigma/\mathrm{d}\Omega=(2\pi^2V|F_H^2|H^2K_BT)/(3v_cM_c)\sum_{j=1}^{2}(j/c_j^2)\times\sum_n\sum_\varepsilon\{q_n^2|1+\beta_j\varepsilon[\xi\mathbf{i}_1+(1-\xi)\mathbf{i}_2]\hat{\mathbf{q}}_n|\}^{-1}, \qquad (13)$$

where β_j denotes the ratio between the sound velocity and the neutron velocity corresponding to the Bragg wavelength:

$$\beta_j=c_jm_n/\hbar k_B=c_j/v_B.$$

$\hat{\mathbf{q}}_n$ is the unit wave vector of the phonon $\mathbf{q}_n$ and k_B is the wave number of Bragg-scattered neutrons.

4. The scattering surface

Equation (10) represents the *scattering surface*. Let us transform (10) in accordance with the approximations used in the previous section.

We shall replace k_1 and k_e by the dimensionless variables x and y:

$$x=(k_1-k_e)/k_e;\quad y=(k_e-k_B)/k_B.$$

The variation over y refers to a TOF scan in the neighbourhood of the Bragg peak, while the variable x describes the energy transfer at scattering. For small energy transfers we have, from (12),

$$\varphi-1\simeq -2x/\xi$$

and (10) becomes

$$q=k_B\varepsilon(x/\xi\beta_j). \qquad (14)$$

If the crystal is oriented with the Bragg vector $\mathbf{H}$ in the horizontal plane, making an angle of $\pi/2+\theta_B$ with the incident beam, the mean direction of the diffracted beam is also horizontal and has the unit vector $\mathbf{i}_{2B}$. Any scattering direction $\mathbf{i}_2$ can be defined with respect to $\mathbf{i}_{2B}$ by the horizontal and vertical angular divergences γ and δ, respectively. Let us suppose that the surface of the position-sensitive detector is perpendicular to $\mathbf{i}_{2B}$. If the horizontal and vertical coordinates are denoted by U_e and V_e, respectively, on this surface, γ and δ are

$$\gamma=2\theta-2\theta_B=(U_e-U_B)/L_2;\quad \delta=(V_e-V_B)/L_2.$$

The dimensionless quantities (y,γ,δ) uniquely define the vector $\mathbf{Q}_e$. Thus, choosing an orthogonal coordinate system $(\mathbf{I},\mathbf{J},\mathbf{K})$ with

$$\mathbf{I}=(\mathbf{i}_1+\mathbf{i}_{2B})/(|\mathbf{i}_1+\mathbf{i}_{2B}|),\quad \mathbf{J}=\mathbf{H}/H,\quad \mathbf{K}=\mathbf{I}\times\mathbf{J},$$

we have

$$\mathbf{Q}_e=2\pi\mathbf{H}+k_B[-\gamma\sin\theta_B\mathbf{I}+(2y\sin\theta_B+\gamma\cos\theta_B)\mathbf{J}+\delta\mathbf{K}].$$

In the same manner, we can write an expression for the phonon wave vector $\mathbf{q}$ as

$$\mathbf{q}=k_B\{[-(x/\xi)\cos\theta_B-\gamma\sin\theta_B]\mathbf{I}+[2(y+x-x/2\xi)\sin\theta_B+\gamma\cos\theta_B]\mathbf{J}+\delta\mathbf{K}\}. \qquad (15)$$

We note that $\mathbf{q}(x=0)=\mathbf{Q}_e-2\pi\mathbf{H}=\mathbf{q}_e$.

By equalizing q^2 from (14) and (15), we now obtain

$$(\beta^2\nu^2-1)(x/\xi)^2-2\beta^2M(x/\xi)+\beta^2N^2=0, \qquad (16)$$

where

$$M=2(\eta-\cos^2\theta_B)y-\zeta\gamma \qquad (17)$$

$$N^2=q_e^2/k_B^2=4y^2\sin^4\theta_B+(\gamma+y\sin 2\theta_B)^2+\delta^2 \qquad (18)$$

$$\eta = 1 - 2\xi \sin^2 \theta_B; \quad \zeta = \xi \sin 2\theta_B; \quad \nu^2 = \eta^2 + \zeta^2. \tag{19a,b,c}$$

The solution of (16) is

$$(x/\xi)_{1,2} = \beta(\beta M \pm \Delta)^{1/2}/(\beta^2\nu^2 - 1) \tag{20}$$

with

$$\Delta = \beta^2 M^2 - (\beta^2\nu^2 - 1)N^2. \tag{21}$$

Equation (16), obtained from the general equation (10), under a set of approximations valid for TDS from low-frequency acoustic phonons, is the scattering surface 'seen' by the TOF diffractometer. It is a quadratic equation between four variables, y, γ, δ and x, and it represents a hyperboloid of two sheets or an ellipsoid in four-dimensional space ($\mathbf{Q}_e$, ω). It is not difficult to understand the nature of this surface. In a given time channel (T_e, U_e; V_e), which uniquely determines the point $\mathbf{Q}_e$, the diffractometer integrates the contribution to the counting rate from all points of the space ($\mathbf{Q}$, ω) situated on a curve Γ passing through $\mathbf{Q}_e$. If the scattering is coherent and inelastic, the cross section is defined only for the points situated on the dispersion surface (DS), a cone of two sheets for every low-energy acoustic mode. These points have $\mathbf{Q}$ different from $\mathbf{Q}_e$ but the contributions to the counting rate are 'seen' as coming from $\mathbf{Q}_e$. The intersection points $\Gamma(\mathbf{Q}_e)$–DS are then projected on a line parallel to the $\hbar\omega$ axis, which passes through $\mathbf{Q}_e$. The scattering surface (16) is obtained from the dispersion surface by this complicated point-by-point projection. In the following, this will be identified as SS4 (scattering surface in four-dimensional space).

Let us cross SS4 with a plane of the space $\mathbf{Q}_e$. A surface in three-dimensional space (SS3) results, one dimension being x, the other two being independent parameters in this crossing plane. By using (15), one obtains a surface in the space of the phonon wave vectors $\mathbf{q}$. This is just the scattering surface described in the papers of Willis (1969, 1970, 1986). By crossing SS4 with a family of parallel planes in $\mathbf{Q}_e$, one obtains a family of SS3s with the same topology for all members. However, different families of planes produce families of SS3s with different topologies. Willis (1986), analysing the SS3 at $\gamma = 2\theta - 2\theta_B$ = constant, found three regions of the parameter β in which the SS3s have different topologies. Popa (1987), making an analysis at $y = (T_B - T_e)/T_B$ = constant, also found three regions for β, different from those of Willis, which become two regions in the limit $\xi \to 0$. There is no contradiction because two different cross sections of the unique SS4 were analysed.

Let us analyse the cross section in the general case. We shall consider the plane P in the space $\mathbf{Q}_e$ to be perpendicular to the plane (γ,y) and at a distance r from the origin. The normal to P is at an angle χ to the γ axis (see Fig. 2). Furthermore, let us denote a variable t along the line of intersection of the planes P and (γ,y). By replacement of the variables γ and y on P by t, the discriminant Δ is written as a quadratic form in the variables t and δ with r and χ as parameters. We look for the regions in plane P where $\Delta \geq 0$ and for this we need the roots t_1, t_2 of the equation $\Delta(t,\delta) = 0$, if they exist, and the quantity μ^2 defined by

$$\mu^2 = (\eta^2 \sin^2 \chi + 4\cos^2 \chi \sin^2 \theta_B \cos^2 \theta_B - \eta \sin 2\chi \sin 2\theta_B) \times (\sin^2 \chi + 4\cos^2 \chi \sin^2 \theta_B - \sin 2\chi \sin 2\theta_B)^{-1}. \tag{22}$$

Taking account of the inequality

$$\nu^2 \geq \mu^2,$$

which is true for any ξ, χ, θ_B, we can now find the topology of the SS3s in the space (x, t, δ). The topology of SS3 in the space $\mathbf{q}$, which corresponds to the plane P, will evidently be the same.

There are three distinct regions of β:

(i) If $0 < \beta < 1/\nu$, solutions $(x/\xi)_{1,2}$ of (16) exist in all points of the plane P, one positive, the other negative. As q in (14) must be positive, the positive solution corresponds to phonon creation and the negative to phonon annihilation [ε = sign (x/ξ)]. SS3 is a hyperboloid of two sheets.

(ii) If $1/\nu < \beta < 1/\mu$, SS3 is also a hyperboloid of two sheets but the range $t_1 < t < t_2$ exists in which the TDS is forbidden. At the left and right of this range, the scattering is with phonon creation only or with phonon annihilation only.

(iii) If $1/\mu < \beta < \infty$, SS3 is an ellipsoid. TDS is allowed in the range $t_1 < t < t_2$ but at the left and right of this range TDS is forbidden.

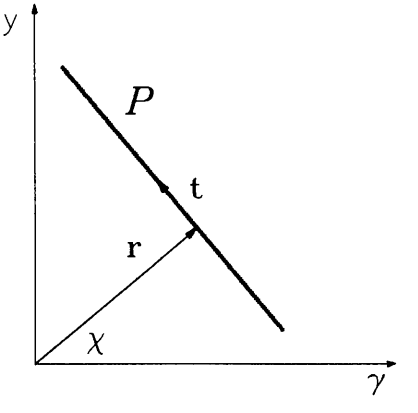

Fig. 2. The scanning plane $P(t, \delta)$. Reciprocal space is scanned at $2\theta - 2\theta_B = r$ if $\chi = 0$ and at $(T_B - T)/T_B = r$ if $\chi = \pi/2$.

The forbidden ranges in both (ii) and (iii) have been observed recently in experiments on barium fluoride by Carlile, Keen, Wilson & Willis (1992).

Special attention must be paid to the cases where $\beta = 1/\nu$ and $\beta = 1/\mu$. When $\beta = 1/\nu$, (16) has only one solution:

$$x/\xi = N^2/2M.$$

SS3 is a hyperboloid of two sheets, as in (i) and (ii), but with one asymptotic plane parallel to the x axis. If $\beta = 1/\mu$, SS3 is a paraboloid.

From this analysis, we note that there are two critical values of β, delimiting the regions with different topologies for SS3:

$$\beta_\nu = 1/\nu \quad \text{and} \quad \beta_\mu = 1/\mu. \tag{23}$$

The first value depends only on ξ and θ_B and, moreover, it becomes unity when $\xi \to 0$; however, the second value depends also on the orientation of the plane of scanning P.

There are two cases of particular interest:

(*a*) For $\chi = 0$, the variable t is just y, the space $\mathbf{Q}_e$ is scanned at a constant offset angle, $\gamma = r$, and $\beta_\mu = 1/\cos\theta_B = \beta_\theta$. This result was discussed by Willis (1986).

(*b*) For $\chi = \pi/2$, the variable t is $-\gamma$, the space $\mathbf{Q}_e$ is scanned at a constant TOF $y = r$ and

$$\beta_\mu = 1/|\eta| = \beta_\eta.$$

If $\xi \to 0$, $\eta \to \nu \to 1$ and $\beta_\eta \to \beta_\nu \to 1$ and there remain only two regions of SS3 with different topologies for a given y, as in the angular-dispersive method. This behaviour is easy to understand because the integration of inelastic processes in TOF, for a given incident wavelength, becomes similar to that for angular-dispersive neutron diffraction if $\xi \to 0$. This result was reported by Popa (1987).

Fig. 3 shows the cross sections, $\delta = 0$, of the two kinds of SS3 at $\gamma = r$ (thin curve) and $y = r$ (thick curve) for the same value of r; the vertical axis is x/ξ and the horizontal axis is y or γ. The same cross sections but in the space $(q_x/k_B, q_y/k_B)$ are shown in Fig. 4. The instrumental parameters used for these figures were $\xi = 0.3$ and $\theta_B = 60°$, giving $\beta_\nu = 1.644$, $\beta_\eta = 1.818$ and $\beta_\theta = 2$. For β we used the value 1.9. For the cross section $\gamma = r$, the value $\beta = 1.9$ lies within region (ii), whereas it is in region (iii) for the cross section $y = r$.

5. Concluding remarks

Once the solutions $(x/\xi)_n$ of (16) are found, it is possible to calculate, using (14), the vectors $\mathbf{q}_n$ that appear in (13) and consequently to perform in this last expression the summation over n and ε, keeping in mind that $\varepsilon = \text{sign}\,(x/\xi)$. One obtains two different expressions for the two regions of β separated by β_ν:

$$\begin{aligned} d\sigma/d\Omega(Q_e) &= (4\pi^2/3)(V/v_c) \\ &\times (|F_H|^2 H^2 K_B T/M_c k_B^2) \\ &\times \sum_{j=1}^{2} (j/c_j^2) S_j(Q_e), \end{aligned} \tag{24}$$

where

$$S_j(Q_e) = \begin{cases} 1/N^2 & \text{for } \beta_j < \beta_\nu \\ \beta_j |M|/N^2 \Delta_j^{1/2} & \text{for } \beta_j > \beta_\nu. \end{cases} \tag{25}$$

For $\beta < \beta_\nu$, S is defined at all points of the space $\mathbf{Q}_e$, but, for $\beta > \beta_\nu$, S is defined only at the points in which $\Delta \geq 0$; these points were identified in the previous section. The function S has an infinite discontinuity at the point $\mathbf{Q}_e = 0$ if $\beta < \beta_\nu$ and at the edges of the allowed regions if $\beta > \beta_\nu$, but these discontinuities are integrable.

The main results reported in this paper can be summarized as follows: (*a*) We have derived, for any

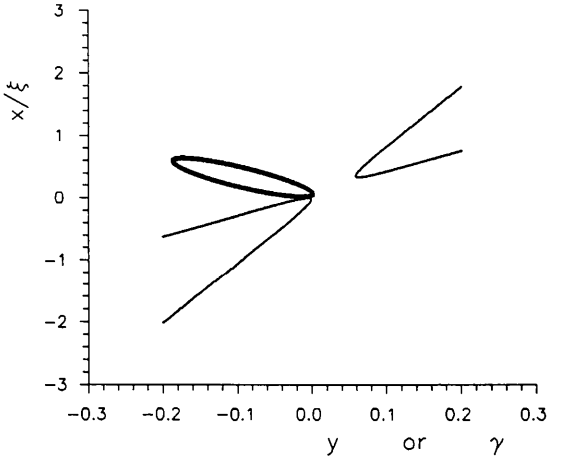

Fig. 3. SS4 cross sections, $\delta = 0$ $\gamma = r$ (thin curve), and $\delta = 0$, $y = r$ (thick curve), calculated using the values $r = 0.01$, $\xi = 0.3$, $\theta_B = 60°$ and $\beta = 1.9$. The horizontal axis is y in the first case and γ in the second case.

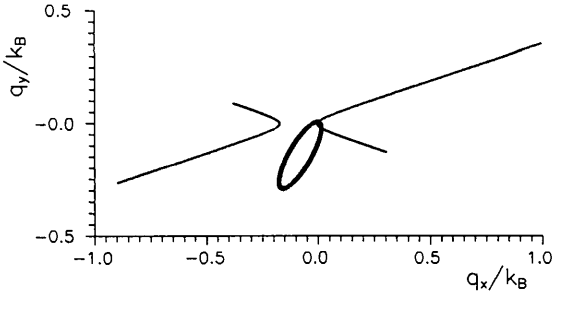

Fig. 4. The cross sections ($q_z = 0$) of SS3 in the space $\mathbf{q}$. The curves correspond to those in Fig. 3. (0,0) is the end point of $2\pi\mathbf{H}/k_B$.

value of the parameter ξ (*i.e.* the ratio of the sample-to-detector flight path and the total flight path), the differential cross section measured in TOF neutron diffractometry. (*b*) For coherent inelastic scattering, this cross section is fully described by the scattering surface in the four-dimensional space ($\mathbf{Q}_e$, ω). (*c*) For scattering by low-frequency acoustic phonons, this surface is defined at every point of the space $\mathbf{Q}_e$ if $\beta < \beta_\nu$ but it is not defined in some regions of this space if $\beta > \beta_\nu$. (*d*) Forbidden ranges exist in both incident wavelengths and scattering angles if $\beta_\nu < \beta < \beta_\mu$; in these ranges, the scattering is allowed if $\beta > \beta_\mu$. (*e*) The value of β_μ depends on the orientation of the scanning plane in the space $\mathbf{Q}_e$. For the particular case of scanning at constant offset from the Bragg scattering angle, β_μ becomes $1/\cos\theta_B$, as reported by Willis (1986). (*f*) Finally, we have found an analytical expression for the differential cross section of scattering by low-energy acoustic phonons. This will be used in a further paper to calculate the TDS correction of the Bragg peaks measured by the TOF diffractometer.

The authors are deeply indebted to Dr C. J. Carlile of the Rutherford Appleton Laboratory, England, for discussions on the contents of this paper.

References

CARLILE, C. J., KEEN, D. A., WILSON, C. C. & WILLIS, B. T. M. (1992). *Acta Cryst.* A**48**, 826–829.
COOPER, M. J. (1971). *Acta Cryst.* A**27**, 148–157.
COOPER, M. J. & ROUSE, K. D. (1968). *Acta Cryst.* A**24**, 405–410.
MARSHALL, W. & LOVESEY, S. W. (1971). *Theory of Thermal Neutron Scattering*. Oxford: Clarendon Press.
POPA, N. C. (1987). Preprint JINR, No. E14-87-180. Joint Institute for Nuclear Research, Dubna, Russia.
WILLIS, B. T. M. (1969). *Acta Cryst.* A**25**, 277–300.
WILLIS, B. T. M. (1970). *Acta Cryst.* A**26**, 396–401.
WILLIS, B. T. M. (1986). *Acta Cryst.* A**42**, 514–525.

Acta Cryst. (1994). A**50**, 63–68

The Half-Widths of Powder Bragg Intensity Profiles Deduced in Reciprocal Space. I. Ideal Powders

BY ELISABETH ROSSMANITH

Mineralogisch-Petrographisches Institut der Universität Hamburg, D-2000 Hamburg 13, *Grindelallee* 48, *Germany*

(*Received* 30 *March* 1993; *accepted* 29 *June* 1993)

Abstract

New formulas for the full widths at half-maxima (FWHMs) of powder Bragg intensity profiles are deduced in reciprocal space, using the concept for the calculation of the peak width introduced for single-crystal diffractometry by Rossmanith [*Acta Cryst.* (1992), A**48**, 596–610]. In paper I, a basic formula for strain-free and preferred-orientation-free powders is deduced. Furthermore, it is shown that comparison of experimental widths with theoretical FWHMs calculated with the new expression results in physically significant values for the particle size in the powder. In a forthcoming paper II, the effect of strain on the FWHM will be analysed.

Introduction

Profile analysis of powder diffraction diagrams requires knowledge of the height, width and distribution function (*i.e.* Gauss, Lorentz, pseudo-Voigt *etc.*) of the intensity profile.

Expressions for the calculation of the resolution functions of *N*-crystal powder spectrometers are given by, for example, Sabine (1987) and Wroblewski (1991). The formulas given by these authors are difficult to handle for two reasons. First, most of the transmission and reflection probability distributions involved in the expressions are not known exactly in routine powder diffraction experiments. Second, evaluation of these expressions requires time-consuming computations of integrals, even if approximations (for example pseudo-Voigt) for the distribution functions are used.

The widths of the Bragg intensity profiles are, therefore, usually calculated using the simplified version of the formula given by Caglioti, Paoletti & Ricci (1958):

$$\Delta 2\theta^2 = U\tan^2\theta + V\tan\theta + W. \qquad (1a)$$

In Rietveld analysis (Rietveld, 1969), the physically meaningless half-width parameters U, V and W are determined by least-squares fitting of calculated to measured FWHMs.